Switch-mediated activation and retargeting of CAR-T cells for B-cell malignancies

David T. Rodgers[a], Magdalena Mazagova[a], Eric N. Hampton[a], Yu Cao[b], Nitya S. Ramadoss[a,1], Ian R. Hardy[a,2], Andrew Schulman[a], Juanjuan Du[a], Feng Wang[a], Oded Singer[a,3], Jennifer Ma[a], Vanessa Nunez[a], Jiayin Shen[a,4], Ashley K. Woods[a], Timothy M. Wright[a], Peter G. Schultz[a,b,5], Chan Hyuk Kim[a,5], and Travis S. Young[a,5]

[a]Department of Biology, California Institute for Biomedical Research, La Jolla, CA 92019; and [b]Department of Chemistry and The Skaggs Institute for Chemical Biology, The Scripps Research Institute, La Jolla, CA 92037

Contributed by Peter G. Schultz, December 11, 2015 (sent for review October 23, 2015; reviewed by Carl H. June and Kevan M. Shokat)

Chimeric antigen receptor T (CAR-T) cell therapy has produced impressive results in clinical trials for B-cell malignancies. However, safety concerns related to the inability to control CAR-T cells once infused into the patient remain a significant challenge. Here we report the engineering of recombinant antibody-based bifunctional switches that consist of a tumor antigen-specific Fab molecule engrafted with a peptide neo-epitope, which is bound exclusively by a peptide-specific switchable CAR-T cell (sCAR-T). The switch redirects the activity of the bio-orthogonal sCAR-T cells through the selective formation of immunological synapses, in which the sCAR-T cell, switch, and target cell interact in a structurally defined and temporally controlled manner. Optimized switches specific for CD19 controlled the activity, tissue-homing, cytokine release, and phenotype of sCAR-T cells in a dose-titratable manner in a Nalm-6 xenograft rodent model of B-cell leukemia. The sCAR–T-cell dosing regimen could be tuned to provide efficacy comparable to the corresponding conventional CART-19, but with lower cytokine levels, thereby offering a method of mitigating cytokine release syndrome in clinical translation. Furthermore, we demonstrate that this methodology is readily adaptable to targeting CD20 on cancer cells using the same sCAR-T cell, suggesting that this approach may be broadly applicable to heterogeneous and resistant tumor populations, as well as other liquid and solid tumor antigens.

chimeric antigen receptor T cell | autologous cell therapy | antibody engineering | cancer | leukemia

Recent clinical studies of chimeric antigen receptor T (CAR-T) cells in heavily pretreated patients with B-cell malignancies have demonstrated sustained remissions. CARs endow patient-derived T cells with the ability to recognize and eliminate cancer cells through a surface-displayed single-chain antibody variable domain (scFv) coupled to intracellular costimulatory and activation domains (1, 2). By linking the specificity of antibody recognition with T-cell–mediated cytotoxicity, CAR-T cells are highly efficacious against antigen-positive tumor cells in an HLA-independent manner. Thus far, the greatest clinical successes have been achieved by targeting the pan–B-cell antigen CD19 (CART-19) in patients with relapsed refractory acute lymphoblastic leukemia (ALL) (3). The success of CART-19 in treating patients who have previously failed treatment with the CD19 bispecific blinatumomab highlights the benefits of genetic engineering approaches that enhance the cellular immune response to tumors (4).

Despite impressive success in early-stage clinical trials, conventional CAR-T cells have limitations associated with the lack of control over their activation and expansion in vivo (5). For example, CAR-T cells undergo rapid proliferation (up to 10^4-fold expansion) upon encountering antigen-positive cells in the patient, which has resulted in serious cases of tumor lysis syndrome (TLS) and fatal cytokine release syndrome (CRS) (6–8). Further complications may be caused by the persistent on-target activity of CAR-T cells. For example, in the case of CART-19, engineered T cells indiscriminately kill malignant and normal B cells, leading to long-term B-cell aplasia (9, 10). Finally, the fixed antigen-specificity of conventional CAR-T cells precludes the targeting of antigen-loss escape mutants, which has recently been shown to be a source of relapse in up to 10% of ALL patients undergoing CART-19 therapy (4, 10–12).

Approaches to improving CAR–T-cell safety have included the use of kill switches that can eliminate CAR-T cells in the case of severe toxicity (13, 14). However, kill switches do not provide control over T-cell activation and expansion, and result in the irreversible elimination of potentially therapeutic CAR-T cells. More recently, a split chimeric receptor has been described that dimerizes in the presence of a small molecule, and thereby provides tunable CAR–T-cell activity (15). However, this approach is still limited by the fixed antigen-specificity of conventional CAR design. Alternatively, strategies that use antibody-based switches to mediate the interaction between the CAR-T cell and target cell enable full control over both activity and specificity (*SI Appendix*, Fig. S1*A*) (16–18). By combining the titratability of antibody-based therapies with the efficacy of genetically modified CAR-T cells, this approach has the potential to prevent CRS and TLS through improved control of the CAR–T-cell

Significance

Chimeric antigen receptor T (CAR-T) cell therapy has produced promising results in clinical trials but has been challenged by the inability to control engineered cells once infused into the patient. Here we present a generalizable method of controlling CAR-T cells using peptide-engrafted antibody-based molecular switches that act as a bridge between the target cell and CAR-T cell. We show that switches specific for CD19 govern the activity, tissue-homing, cytokine release, and phenotype of switchable CAR-T cells in a dose-titratable manner using xenograft mouse models of B-cell leukemia. We expect that this method of tuning CAR-T cell responses will provide improved safety and versatility of CAR–T-cell therapy in the clinic.

Author contributions: D.T.R., T.M.W., P.G.S., C.H.K., and T.S.Y. designed research; D.T.R., M.M., E.N.H., Y.C., N.S.R., I.R.H., A.S., O.S., J.M., V.N., J.S., and A.K.W. performed research; J.D. and F.W. contributed new reagents/analytic tools; T.M.W., P.G.S., C.H.K., and T.S.Y. analyzed data; and D.T.R., P.G.S., and T.S.Y. wrote the paper.

Reviewers: C.H.J., University of Pennsylvania; and K.M.S., University of California, San Francisco.

The authors declare no conflict of interest.

Freely available online through the PNAS open access option.

[1]Present address: Shriram Center, Stanford University, Stanford, CA 94305.

[2]Present address: Fate Therapeutics, San Diego, CA 92121.

[3]Present address: Viral Vector Core, Weizmann Institute of Science, Rehovot 76100, Israel.

[4]Present address: Department of Infectious Diseases, Shanghai Public Health Clinical Center, Fudan University, Shanghai 201508, China.

[5]To whom correspondence may be addressed. Email: schultz@scripps.edu, chkim@calibr.org, or tyoung@calibr.org.

This article contains supporting information online at www.pnas.org/lookup/suppl/doi:10.1073/pnas.1524155113/-/DCSupplemental.

activation. The modularity of such an approach allows targeting of a broader range of antigens by a single switchable CAR-T (sCAR-T) cell, which may be an effective strategy for addressing antigen-loss relapse mutations and heterogeneous tumors.

Here we describe a method of switch-mediated activation and retargeting of CAR-T cells in which antibody-based switches are engineered by the introduction of peptide neo-epitopes (PNE) at defined locations in an antigen-specific antibody. The sCAR-T cell binds the PNE and no endogenous tissue or antigen, and is therefore strictly dependent on the presence of the switch for activation. We show that this approach affords control over the geometry of the immunological synapse between the sCAR-T cell, switch, and target cell, and allows rapid optimization of activity, which results in excellent potency in vitro and in vivo that is comparable to a conventional CAR-T cell. Given the breadth of prior research on CART-19, along with the need for a solution to the CRS and long-term B-cell aplasia associated with its clinical use, we initially developed this methodology in the context of CD19-expressing B-cell malignancies. However, we also show that this approach is readily adaptable to target CD20-expressing cells, suggesting that sCAR-T cells may be applicable to a wide-range of tumor antigens.

Results

Design of an Orthogonal sCAR-T Cell. A 14-aa PNE sequence from the yeast transcription factor GCN4 was chosen as the target of the sCAR. This sequence does not occur in the human proteome and thereby provides an orthogonal interaction between the sCAR-T cell and switch. Moreover, high-affinity antibodies against this peptide have been previously developed by directed evolution (19–21). To determine the risk of immunogenicity associated with engraftment of this nonhuman sequence into an antibody fragment (Fab) to create a switch, we performed an in silico immunogenicity analysis of the PNE linked to the N terminus of the light or heavy chains of a model, therapeutically approved antibody (Herceptin) (*SI Appendix*, Fig. S1*B*). This analysis predicted the PNE graft to have a low probability of inducing an antibody response in the context of a prototypical antibody and supported its use in generating switches. To generate switch molecules specific for the CD19 antigen, the PNE was introduced at defined sites in the anti-CD19 antibody FMC63 (22). This antibody clone is used in the most widely studied conventional CART-19 construct in clinical trials and thus provides a direct comparison for the sCAR–T-cell system (23). By varying the stoichiometry and site of PNE engraftment in FMC63, we could systematically vary the valency and orientation of the

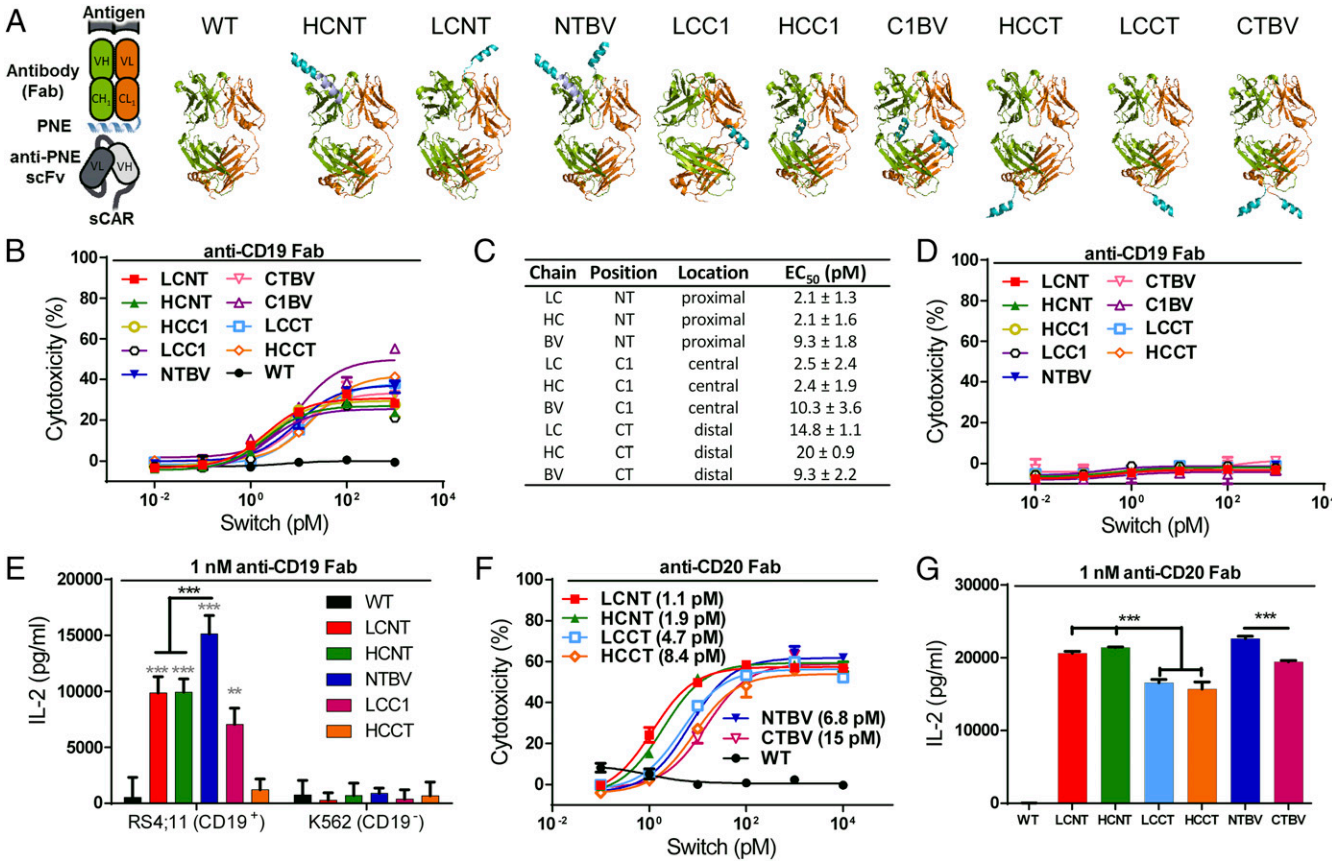

Fig. 1. Relative orientations and in vitro activity of switches. (*A*) Schematic depicting the immunological synapse between the sCAR, switch, and antigen (*Left*); ribbon diagrams depicting the different switch designs (*Right*), where the light chain is shown in gold, heavy chain in green, and PNE in blue; the rigid linker on HCNT is shown in gray. The diagrams are oriented such that the antigen-binding interface is at the top. (*B*) Cytotoxicity of sCAR-T cells against $CD19^+$ RS4;11 cells with titration of anti-CD19 Fab switch molecules. Corresponding IgG designs are shown in *SI Appendix*, Fig. S5*A*. (*C*) Table of EC_{50} values of cytotoxicity from *B*. (*D*) Cytotoxicity of sCAR-T cells against $CD19^-$ K562 cells with the anti-CD19 Fab switch molecules. Corresponding IgG switches are shown in *SI Appendix*, Fig. S5*B*. (*E*) IL-2 released from sCAR-T cells cultured with RS4;11 or K562 and 1-nM anti-CD19 Fab switches. Gray asterisks denote significance compared with wild-type switch and black asterisks denote significance between switches. (*F*) Cytotoxicity of sCAR-T cells against $CD20^+$ Raji cells with the anti-CD20 Fab switch molecules. (*G*) IL-2 released from sCAR-T cells cultured with Raji cells and 1 nM anti-CD20 Fab switches. All assays were performed with effector to target (E:T) = 10:1 and 24 h incubation. Cytotoxicity was assessed by LDH release. Data are represented as mean ± SD. Where listed, values next to switches show EC_{50} of cytotoxicity. Significance was calculated using the Student's *t* test, where $^{**}P < 0.01$ and $^{***}P < 0.001$.

antigen-binding region of the antibody switch relative to the scFv on the T-cell surface (Fig. 1*A* and *SI Appendix*, Fig. S1*A*). Four fusions of the PNE were generated by linking the PNE to the N or C terminus (NT or CT, respectively) of the heavy or light chains (HC or LC, respectively) of the Fab with short peptide linkers. We found that a GGGGS linker was suitable in all positions except for fusion to the N terminus of the heavy chain (HCNT), which afforded increased yields with a putative helical forming EAAAK sequence motif (24) (*SI Appendix*). In addition, we inserted the PNE directly into loops of the constant region 1 (C1) in the center of the heavy and light chains using a strategy similar to one we had previously developed for direct peptide-antibody loop fusions (25–27). These C1 constructs provided yet another distinct binding orientation of the sCAR relative to the target antigen, which could be preferable for certain antibody epitopes on target antigens. Finally, the PNE was engrafted into both the heavy and light chains to create bivalent switches (NTBV, CTBV, C1BV). The PNE-engrafted switch molecules were efficiently expressed in Fab and IgG format using transient transfections in HEK cells, with yields 50–100% that of wild-type FMC63 antibody (*SI Appendix*, Fig. S2 *A* and *B*). Engraftment of the PNE at all sites in the Fab had minimal impact on protein stability and antigen binding as determined by thermal melt assays (*SI Appendix*, Fig. S3*A*) and flow cytometry-based binding to $CD19^+$ RS4;11 (EC_{50} = 5.6 nM ± 6.3) (*SI Appendix*, Fig. S3*B*), respectively.

To create a sCAR-T cell that recognizes the switch, a sCAR was developed using the 52SR4 antibody, which selectively binds the PNE with high affinity (K_d = 5.2 pM, reported) (21). The 52SR4 scFv was incorporated into a second generation CAR construct harboring the human CD8 hinge (spacer), CD8 transmembrane, 4-1BB costimulatory, and CD3ζ activation domains. This design is identical to the second generation CAR used by June and coworkers in CART-19 (28). Lentiviral transduction of this construct into freshly isolated human PBMCs demonstrated efficient surface expression with transduction efficiencies of 50–75%, which were comparable to the FMC63-based CART-19 (29) (*SI Appendix*, Fig. S4*A*). Switches bound to sCAR-T cells and not to untransduced T cells (*SI Appendix*, Fig. S4*B*), demonstrating that the sCAR–T-cell–switch interaction is highly specific.

Site and Valency of PNE Engraftment Affects sCAR–T-Cell Potency in Vitro. To empirically determine the optimal switch design for CD19, we tested the potency of each switch in vitro. All switches elicited dose-dependent lysis of $CD19^+$ RS4;11 cells in the presence of sCAR-T cells at picomolar concentrations (Fig. 1 *B* and *C* and *SI Appendix*, Fig. S5*A*). There was a clear structure activity relationship between cytotoxicity and the location of the PNE in the antibody. Switches with the PNE engrafted proximal to the antigen binding site (LCNT, HCNT, NTBV) were generally more potent than switches with the PNE engrafted at the C1 (LCC1, HCC1, C1BV) or C terminus (LCCT, HCCT, CTBV) of the Fab region. No significant lysis of $CD19^-$ K562 cells was observed for any Fab or IgG switch design, even at concentrations 10^3-fold higher than the EC_{50} (Fig. 1*D* and *SI Appendix*, Fig. S5*B*). In addition, wild-type anti-CD19 Fab and IgG lacking the PNE peptide did not induce significant cytotoxicity, demonstrating a strict requirement for PNE-mediated immunological synapse formation. We chose to further pursue switches in the Fab format rather than IgG because the Fab has a shorter pharmacokinetic half-life, which we predicted would enable greater temporal control over the response in vivo.

Consistent with the cytotoxicity results, all switches induced robust IL-2 release (Fig. 1*E*), with the N-terminal PNE switches providing greater IL-2 responses than the constant region or C-terminal PNE switch molecules. Notably, the NTBV switch induced the greatest IL-2 production against RS4;11 cells, indicating a potential benefit of engagement of two sCARs with one switch. Again, addition of the switches did not stimulate cytokine release in the presence of sCAR-T cells and $CD19^-$ K562 cells, confirming that switch binding to the sCAR-T cell alone is not sufficient for activation (Fig. 1*E*). Consistent with the cytokine release data, markers of T-cell activation ($CD25^+$, $CD69^+$) on sCAR-T cells were only up-regulated by the switches in the presence of $CD19^+$ RS4;11 cells and not $CD19^-$ K562 cells (*SI Appendix*, Fig. S5*C*). These results clearly demonstrate that sCAR–T-cell effector function, as measured by activation, cytokine production, and target cell killing, is dependent on the presence of both a target antigen and switch.

To determine whether the same sCAR-T cell could be used to target other antigens relevant to B-cell malignancies, a similar panel of switches was constructed to bind CD20-expressing cancer cells based on the anti-CD20 antibody Ofatumumab (OFA) (*SI Appendix*, Fig. S2*C*) (30). Along with CD19, CD20 is an important pan–B-cell marker and the most widely targeted B-cell antigen in the clinic. To develop the anti-CD20 switch, the OFA antibody was chosen because it binds a membrane proximal epitope (31), which might lead to enhanced activity because of the close association of the T cell and cancer cell. Switches were generated in a fashion similar to the CD19 switches. Consistent with the trend for FMC63, N-terminal PNE switches were found to be more cytotoxic than C-terminal PNE switches (EC_{50} = 1.1–6.8 pM vs. 4.7–15 pM, respectively) against $CD20^+$ Raji cells (Fig. 1*F*). In addition, anti-CD20 N-terminal PNE switches stimulated higher levels of cytokine release than C terminus PNE switches (Fig. 1*G*).

Optimization of the sCAR Design Improves Activity in Vitro. We hypothesized that the increased activity of switches with the PNE engrafted proximal to the antigen binding domain was the result of a decreased overall distance between the sCAR-T cell and target cell (32). To determine whether the distance could be further shortened to increase activity, we modified the hinge region of the sCAR itself (also referred to as the spacer domain), which connects the anti-PNE scFv to the transmembrane domain of the sCAR. The initial sCAR design used a 45-aa CD8-based hinge identical to that of conventional CART-19. To test a shorter hinge, this region of the sCAR was replaced with a 12-aa sequence derived from the hinge of IgG4 (*SI Appendix*, *SI Methods* and Fig. S6*A*). As expected, the IgG4-hinge–based sCAR-T cells had increased cytotoxicity in the presence of the LCNT switch against RS4;11 cells compared with CD8-hinge–based sCAR-T cells (Fig. 2*A*), while retaining antigen specificity for $CD19^+$ cells (Fig. 2*B* and *SI Appendix*, Fig. S7*A*).

We also hypothesized that the increased cytokine induction observed with the bivalent NTBV switch reflected an effect of increased valency on sCAR–T-cell activation. To test whether this notion could be translated to the IgG4 sCAR design, a serine-to-proline mutation [S228P relative to the IgG4 molecule (33)] was incorporated in the IgG4 hinge to enhance interchain sCAR disulfide formation (IgG4m) (*SI Appendix*, Fig. S6*A*). Consistent with previous reports, Western blot analysis confirmed that the sCAR and CART-19 CD8-based hinges formed spontaneous disulfide dimers in the absence of CAR stimulation (*SI Appendix*, Fig. S6*B*) (34). Dimers also formed for the IgG4m-based sCAR hinge containing the S228P mutation, but not for the IgG4 hinge lacking this mutation. As expected, the maximum cell lysis and EC_{50} of cytotoxicity of the IgG4m sCAR against RS4;11 cells with the LCNT switch were increased compared with the IgG4 sCAR lacking the S228P mutation (Fig. 2*A*). This result is consistent with Riddell and coworkers, in which the same IgG4m hinge design increased the activity of anti-ROR1 conventional CAR-T cell compared with other hinge designs in their study (35, 36). However, no corresponding monomeric IgG4 hinge was compared in that study. Thus, our result supports that the S228P

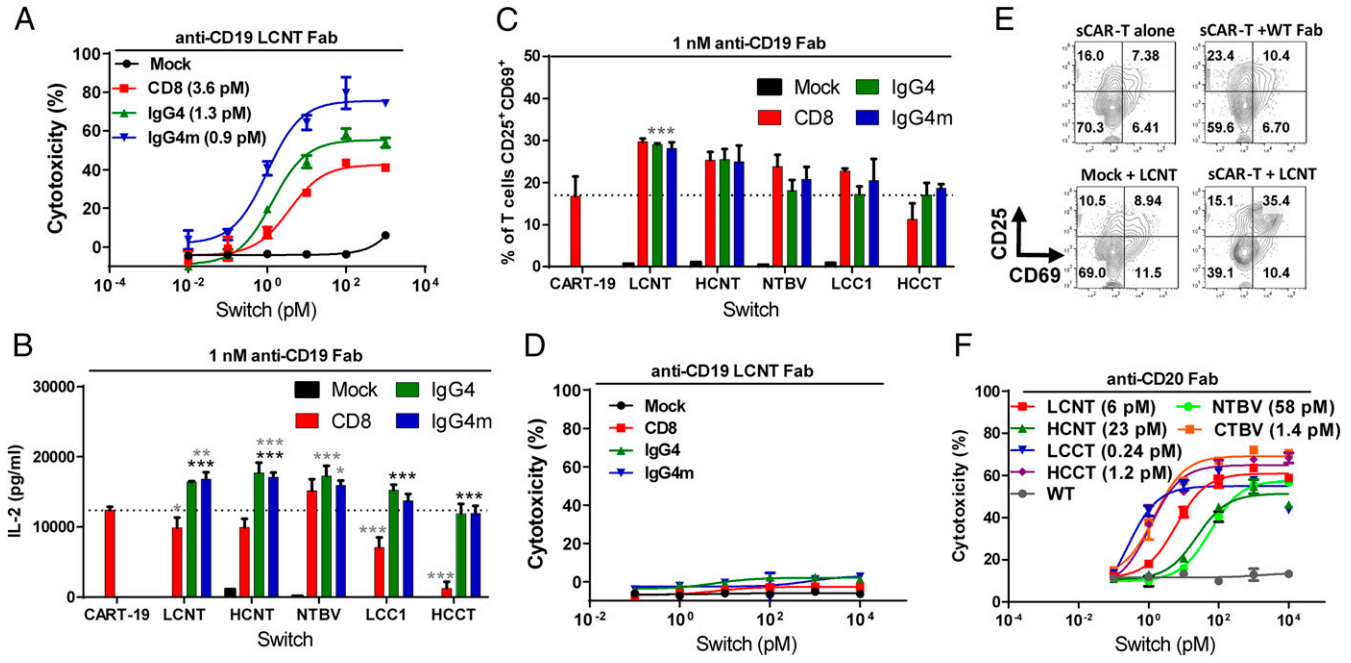

Fig. 2. Activity of sCAR hinge designs. (*A*) Cytotoxicity of sCAR-T cells with CD8, IgG4, or IgG4m hinges, or nontransduced T cells (mock) against $CD19^+$ RS4;11 cells with titration of the anti-CD19 LCNT switch molecule. (*B*) IL-2 released from sCAR-T cells cultured with RS4;11 cells and 1-nM anti-CD19 Fab switches; gray asterisks denote significance between CART-19 and sCAR-T cells and black asterisks denote significance between sCAR–T-cell hinges; mean values for CART-19 is indicated by dotted horizontal line. (*C*) Quantification of the T-cell activation assay in the presence of 1 nM of each anti-CD19 Fab switch. (*D*) Cytotoxicity as described in *A* against $CD19^-$ K562 cells. (*E*) Activation of sCAR-T cells with IgG4m hinge or mock cells in the presence of RS4;11 cells with or without 1-nM LCNT Fab switch measured by flow cytometry with staining for CD25 and CD69. (*F*) Cytotoxicity of sCAR-T cells against $CD20^+$ Raji cells with titration of anti-CD20 Fab switch molecules. Values listed next to switches show EC_{50} of cytotoxicity. All cytotoxicity and cytokine assays were performed with E:T = 10:1 and 24 h incubation. Cytotoxicity was assessed by LDH release. Data are represented as mean ± SD, and statistical significance was calculated using the one-way ANOVA with Tukey's posttest (*B* and *D*), where $*P < 0.05$, $**P < 0.01$, and $***P < 0.001$.

mutation in the IgG4 hinge confers increased sCAR–T-cell activation through dimerization of the sCAR.

We next determined the additive effect of switch and hinge design on sCAR activity, and compared this with conventional CART-19. Each switch design was empirically tested in combination with each hinge design in dose–response for cytotoxicity, cytokine release, and up-regulation of activation markers in the presence of RS4;11 cells. As expected, the observed trend was that cytotoxicity increased as the PNE engraftment site moved from the C-to-N terminus and as the hinge design was shortened from the 45-aa CD8 design to the 12-aa IgG4 design; this was further increased with the IgG4m design (Fig. 2*A* and *SI Appendix*, Fig. S7*A*). Correspondingly, IL-2 release with 1-nM switch was greater with the N-terminal PNE switches (HCNT, LCNT, NTBV) and the IgG4 and IgG4m hinges than with the C-terminal PNE switches (HCCT, LCCT, NTCT) and CD8 hinge (Fig. 2*B*). The NTBV switch increased IL-2 production from CD8 sCAR-T cells by 50% but did not have a significant impact on sCAR-T cells harboring the IgG4 or IgG4m hinges. We expect this may be a result of steric clashes with the shorter IgG4 and IgG4m hinges, which prevent binding of two sCARs to two N-terminal PNEs on one bivalent switch molecule. The trend in switch design on the up-regulation of T-cell activation markers was similar to that observed for cytotoxicity and cytokine production, with the greatest activation observed in response to the LCNT switch (Fig. 2*C*). Collectively, the LCNT switch with the IgG4m sCAR-T cell demonstrated the greatest cytotoxicity compared with other switch/hinge designs and afforded cytokine release and up-regulation of T-cell activation markers that were significantly greater against $CD19^+$ RS4;11 cells.

Specificity of sCAR–T-cell activation is a critical design consideration for switch-based control. Therefore, to confirm that the improved activity of the IgG4m sCAR did not sacrifice specificity, we repeated the assays above on $CD19^-$ K562 cells. The IgG4m sCAR did not cause significant lysis of K562 cells with up to 10 nM of any switch molecule (Fig. 2*D* and *SI Appendix*, Fig. S8 *A* and *B*), nor did the IgG4m sCAR produce IL-2 in the presence of K562 cells and any of the switches (*SI Appendix*, Fig. S8*C*). Furthermore, the IgG4m sCAR-T cells did not exhibit significant up-regulation of activation markers compared with nontransduced (mock) cells in the absence of the PNE-engrafted switch and target antigen (Fig. 2*E*). Taken together, these data confirmed that the improved activity of the IgG4m sCAR did not result in antigen-independent activation. Finally, the activity of sCAR-T cells on RS4;11 cells could be fully inhibited by the addition of an excess of soluble, synthetic PNE peptide, further demonstrating the requirement of a switch for activity (*SI Appendix*, Fig. S8*D*).

To test whether the improved IgG4m hinge design extends to the anti-CD20 OFA switches, we tested the anti-CD20 switches with IgG4m sCAR-T cells on $CD20^+$ Raji cells. As expected, cytotoxicity was increased with the IgG4m sCAR for all CD20 switches compared with CD8 sCAR-T cells (Fig. 2*F*). Unexpectedly, however, the trend in anti-CD20 switch design with the IgG4m sCAR was opposite to what was observed with the CD8 sCAR (Fig. 1*G*). In this case the C-terminal PNE switches were 10- to 100-fold more potent than the N-terminal PNE switches. We hypothesized that this is because of the membrane proximal epitope of the OFA on CD20, which may require additional distance between the PNE and antigen-binding interface of the Fab when the hinge region of the sCAR is short, to alleviate steric clashes at the immunological synapse. Collectively the above studies demonstrate that the activity of sCAR-T cells

can be significantly enhanced through both sCAR hinge and switch design and underscore the advantages of being able to optimized each.

Switch and Hinge Design Effects on Tumor Clearance in Vivo. To investigate the activity of sCAR-T cells in vivo, we evaluated tumor regression in a xenograft model of B-cell leukemia using luciferized human B-ALL Nalm-6 cells in immunodeficient NOD.Cg-*Prkdc*^{scid} *Il2rg*^{tm1Wjl}/SzJ (NSG) mice. In this model, mice without treatment succumb to disease within 21 d. First, to understand the impact of CAR hinge design on in vivo efficacy, mice were inoculated with Nalm-6, followed by intravenous injection of CD8, IgG4, or IgG4m sCAR-T cells 6 d later (*SI Appendix*, Fig. S9*A*). Based on our in vitro results, we chose the anti-CD19 LCNT switch to test in this model. This switch was dosed intravenous (0.5 mg/kg) every other day for 10 d and tumor regression was followed by in vivo imaging (IVIS) of the luciferase signal from Nalm-6 cells (Fig. 3*A*). In line with the in vitro data, both IgG4 and IgG4m sCAR-T cells afforded a significant decrease in tumor burden, whereas CD8 sCAR-T cells had minimal impact on disease compared with untreated controls (Fig. 3*B*). Increased T-cell counts in the peripheral blood at day 17 corresponded with reduced tumor burden and revealed that the IgG4m sCAR-T cells provided significantly greater T-cell expansion compared with the IgG4 or CD8 hinge designs (Fig. 3*C*). Based on this result, the IgG4m sCAR construct was chosen for further in vivo analysis.

Next, we determined the effect of switch graft position and valency on in vivo efficacy. As with the previous model, IgG4m sCAR-T cells were injected 6 d after tumor inoculation and mice were treated every other day (starting at day 6) with the LCNT, HCNT, NTBV, LCC1, or HCCT switches (0.5 mg/kg) (Fig. 3*D*). Analogous to the in vitro data, the N-terminally grafted switches (LCNT, HCNT, and NTBV) afforded the greatest reduction in tumor burden, whereas switches with the PNE at the middle (LCC1) or C terminus (HCCT) provided little control (Fig. 3*E*). T-cell counts at day 20 correlated with reduction of tumor burden and indicated the LCNT switch provided the greatest T-cell expansion (Fig. 3*F*). In agreement with our in vitro data, the combination of the LCNT switch with the IgG4m sCAR resulted in the greatest efficacy in vivo and thus was used in subsequent studies to explore the effect of switch-dosing regimen.

Clearance of Nalm-6 with the IgG4m sCAR-T cell and the LCNT switch in the above model was observed to occur rapidly during the first 96 h of treatment. To further investigate IgG4m sCAR T-cell proliferation and localization during this time interval, Nalm-6 engrafted NSG mice were sorted into four groups and were treated with IgG4m sCAR-T cells (with or without the LCNT switch), conventional CART-19 (with no switch), or no cells. Each group was divided into five cohorts per treatment regimen, which were analyzed at 8, 24, 48, 72, and 96 h after T-cell infusion. Daily dosing of the LCNT switch (0.5 mg/kg) reduced tumor burden within 24 h and continued to shrink the tumor to the limit of luminescence detection (~10^3–10^4 p/s/cm^2/sr) within 96 h (Fig. 4*A*). The rate of clearance during this time was not significantly different from CART-19 (Fig. 4*B*). Human IL-2 in peripheral blood peaked at similar levels at 24 h for CART-19 and at 48 h for sCAR-T cells, and decreased as tumor was cleared (Fig. 4*B*). As expected, IgG4m sCAR-T cells in the absence of switch had no effect on disease progression in this

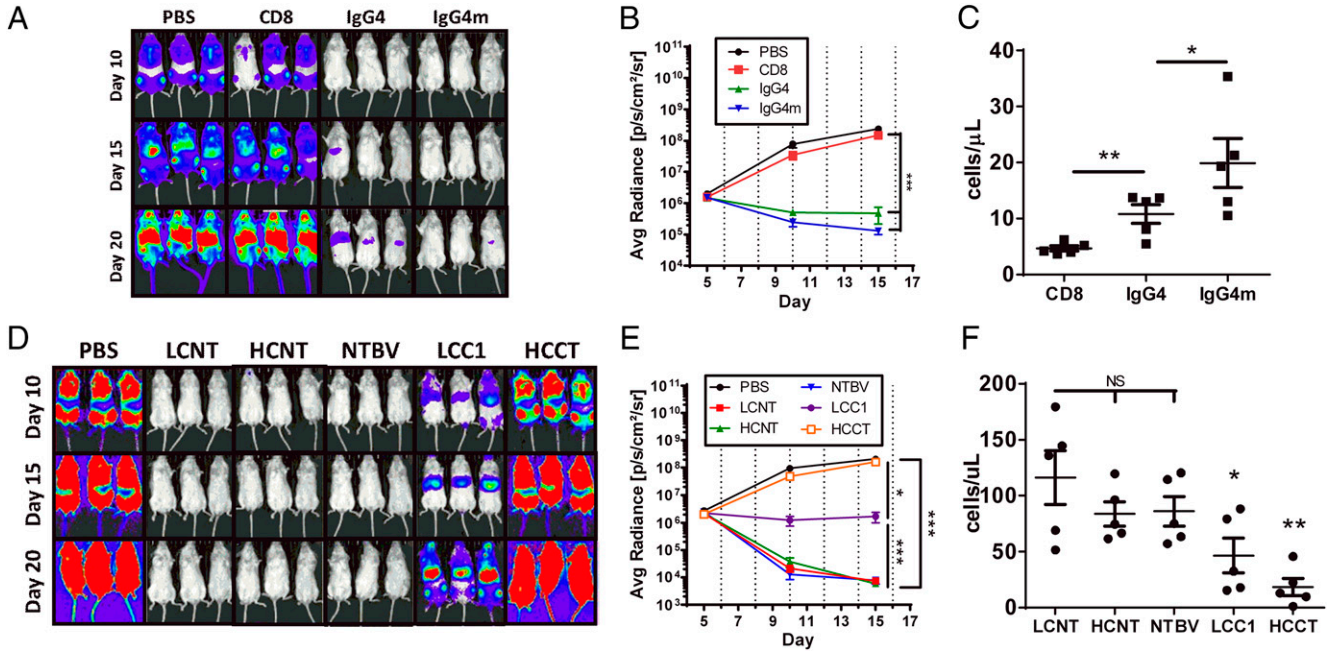

Fig. 3. In vivo activity of switch and hinge designs in Nalm-6 xenograft model. NSG mice were inoculated with CD19$^+$ Nalm-6 cells. After 6 d the mice were injected with luciferin and imaged on an IVIS before being randomly sorted into groups ($n = 5$) with representative tumor burden. Next, 40×10^6 sCAR-T cells with a transduction efficiency of 50–75% were infused intravenously and switch-dosing commenced every other day at 0.5 mg/kg for 10 d. Tumor burden was followed by IVIS. (*A*) Representative IVIS images depicting three of the mice from each of the groups treated with the CD8, IgG4, or IgG4m sCAR-T cells and LCNT Fab switch are shown. (*B*) Quantified tumor burden (as average radiance from luciferase activity from each mouse) from *A* during switch-dosing period ($n = 5$). (*C*) Enumeration of T cells in peripheral blood from *A* at day 17 by flow cytometry using CountBright Beads (Thermo). (*D*) Representative IVIS images depicting three of the mice from each of the groups treated with the IgG4m sCAR-T cells and the anti-CD19 Fab switch designs indicated. (*E*) Quantified tumor burden from *D* during the switch-dosing period ($n = 5$). (*F*) Enumeration of T cells in peripheral blood from *D* at day 20 by flow cytometry as in *C*. Asterisks indicate significance from LCNT Fab group. Data are represented as mean ± SEM, and statistical significance was calculated using the two-way ANOVA with Bonferroni's posttest (*B* and *E*) (shown for final time-point only) or by one-tailed Student's *t* test (*C* and *F*), where $*P < 0.05$, $**P < 0.01$, and $***P < 0.001$; ns, not significant.

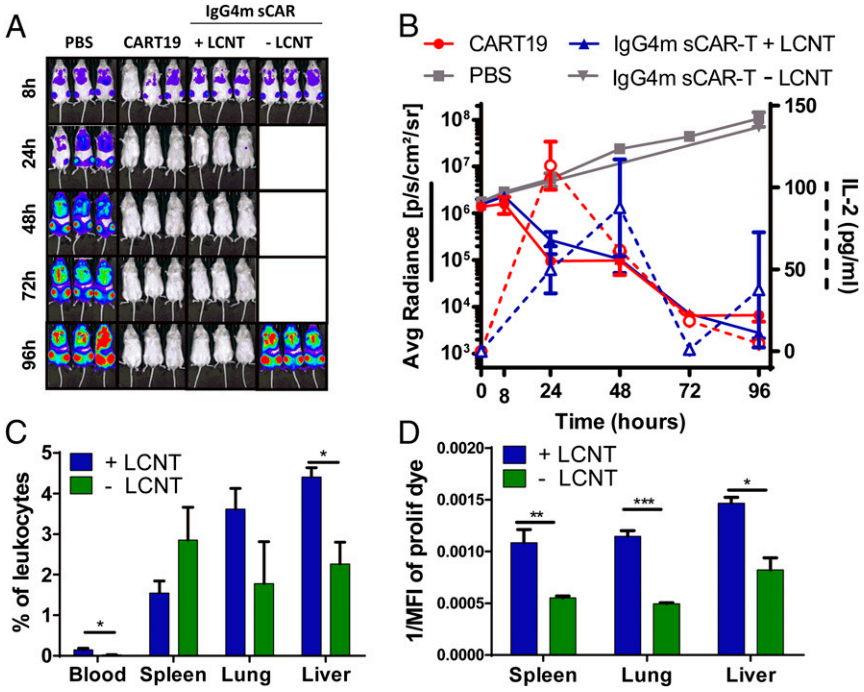

Fig. 4. sCAR–T-cell expansion and localization during tumor clearance. NSG mice were inoculated with Nalm-6 as described in Fig. 3. (*A*) After 6 d, mice were sorted into four groups. Three groups containing five cohorts of mice with representative tumor burden before being injected intravenously with 40×10^6 CART-19, IgG4m sCAR-T cells with (+) LCNT Fab switch, or no T cells (PBS group). A fourth group consisted of two cohorts ($n = 3$) of mice injected intravenously with IgG4m sCAR-T cells without (–) LCNT Fab switch were analyzed at 8 h and 96 h only. LCNT Fab dosing (0.5 mg/kg) in the (+) group was started with initial T-cell infusion and continued daily for 5 d. Luminescence was measured at 8 h and subsequently every 24 h, as indicated. All cells were labeled with eFluor 450 cell proliferation dye before injection. (*B*) Quantified tumor burden (radiance, left axis, solid line) and quantified human IL-2 (pg/mL, right axis, dashed line) in peripheral blood from each cohort shown in *A* at each time point. Gray lines indicate tumor burden in PBS and IgG4m sCAR–T-cell –LCNT Fab controls. (*C*) The proportion of leukocytes that were human $CD3^+CD4/8^+$ in the blood, spleen, lungs and liver at 96 h in the +LCNT and –LCNT groups was quantified by flow cytometry. (*D*) Relative proliferation of T cells in the spleen, lung, and liver at 96 h in +LCNT and –LCNT Fab groups, determined by eFluor 450 dye dilution shown as 1/mean fluorescence intensity. Data are represented as means ± SEM, and statistical significance was calculated using the one-tailed Student's *t* test (*C* and *D*), where $*P < 0.05$, $**P < 0.01$, and $***P < 0.001$.

model, confirming requirement of switch dosing for in vivo antitumor effect. We also tracked IgG4m sCAR-T cells and tumor in the spleen, lung, liver, and peripheral blood by flow cytometry over the 96 h. During this time, Nalm-6 cells were only detectable in the lung and liver (*SI Appendix*, Fig. S9*A*). Correspondingly, significantly increased levels of sCAR-T cells were found in the lung and liver at 96 h in mice dosed with the LCNT switch compared with mice not treated with switch (Fig. 4*C*). Switch dosing did not increase sCAR–T-cell recruitment to the spleen where tumor burden was not detectable. In the organs assessed, sCAR-T cells had proliferated significantly more in the mice treated with LCNT switch (by dye dilution experiments) compared with no switch treatment, again demonstrating the requirement for the switch for sCAR–T-cell expansion (Fig. 4*D* and *SI Appendix*, Fig. S9*B*). The magnitude of sCAR–T-cell proliferation when dosed with the LCNT switch was comparable to that of CART-19 in both the liver and lung (*SI Appendix*, Fig. S9*C*). Taken together, these results indicate that the IgG4m sCAR-T cells dosed with the LCNT switch can expand and eliminate tumor burden with comparable efficacy to conventional CART-19.

Dose-Dependent Control of sCAR–T-Cell Activity in Vivo. To determine the minimal dose frequency required for a sustained response with the IgG4m sCAR-T cells, we tested every day, every other day, or every fifth day dosing of the LCNT switch (0.5 mg/kg) for 15 d in the Nalm-6 model. Every day and every other day dosing yielded comparable rates of tumor regression, which was sustained for >100 d after dosing was discontinued (Fig. 5*A* and *SI Appendix*, Fig. S10*A*). Mice that died between days 40 and 100 (open circles) had no evidence of disease; expiration in these cases was attributed to xenogeneic graft vs. host disease caused by human T cells in the NSG mouse, as previously described (37). Dosing every fifth day (three total dosages) greatly decreased and stabilized disease burden at a low level, but did not completely clear disease based on luciferase signal. This finding corresponds with the expected short half-life for the Fab-based switch in the mouse. Residual disease in this group relapsed when dosing was discontinued indicating that the activity of the sCAR-T cells toward the Nalm-6 cells had been turned "off" in the absence of the switch; nevertheless sCAR-T cells were still detectable in blood up to 64 d after injection (*SI Appendix*, Fig. S10*B*).

Control of cytokine production in vivo is important to prevent CRS in patients receiving CAR–T-cell therapy. To investigate the potential of switch-regulated IgG4m sCAR-T cells to achieve reduced cytokine release in vivo, we correlated switch dosage with cytokine release by the IgG4m sCAR-T cells in the Nalm-6 model. Mice dosed everyday with 0.05, 0.5, or 2.5 mg/kg of the LCNT switch showed a dose-dependent increase in serum IL-2, IFN-γ, and TNF-α at 24 h (Fig. 5*B*) that correlated with dose-dependent reductions in tumor burden by day 10 (Fig. 5*C*). Cytokine production in the 0.5- and 2.5-mg/kg groups was not significantly different from CART-19 at 24 h for all cytokines, except for serum TNF-α, which was decreased in the 2.5-mg/kg group compared with CART-19. However, all cytokines in the 0.05-mg/kg group were significantly lower than CART-19.

To determine if treatment with the lower dose of 0.05 mg/kg could be efficacious, despite lower levels of cytokine production,

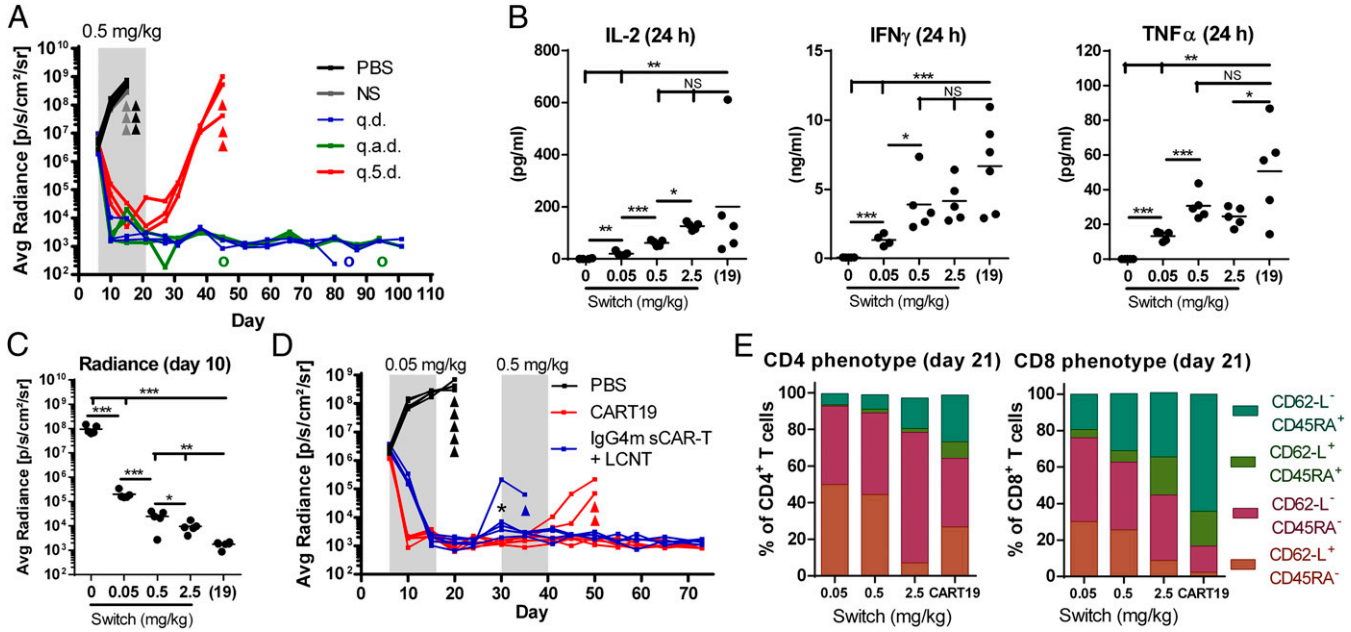

Fig. 5. Influence of switch dosing regimen on sCAR–T-cell activation and efficacy. NSG mice ($n = 3$) were inoculated with Nalm-6 and 6 d later were engrafted with IgG4m sCAR-T cells (transduction efficiency and CD4:CD8 ratio of injected cells: 60%, 1:1.23) as described in Fig. 3. (*A*) Quantified tumor burden from groups dosed every day (q.d.), every other day (q.a.d.), or every fifth day (q.5.d.) with 0.5 mg/kg LCNT. Dosing was carried out for 15 d starting at day 6 (corresponding with IgG4m sCAR–T-cell infusion), as indicated by gray shading (day 6–21). The NS group received IgG4m sCAR-T cells and injections of PBS. Open circles denote the death of individual mice without evidence of tumor burden and likely reflect graft vs. host disease. Triangles in the q.5.d. group indicates mouse expiration because of increasing tumor burden ($n = 3$). (*B*) Levels of IL-2, IFN-γ, and TNF-α at 24 h after first dose, from groups dosed every day with 0, 0.05, 0.5, or 2.5 mg/kg of LCNT. CART-19 is labeled as "(19)" ($n = 5$). (*C*) Quantified tumor burden by IVIS from groups in *B* after 10 d. (*D*) Quantified tumor burden from mice dosed with 0.05 mg/kg LCNT for 10 d indicated by gray shading (day 6–16). Dosing was resumed at 0.5 mg/kg when the average tumor burden in group became significantly higher than CART-19 control at day 30, indicated by an asterisk and second gray shading (day 30–40). Triangles indicate the death of individual mice with significant tumor burden ($n = 5$). Transduction efficiency and CD4:CD8 ratio of injected cells: CART19 = 68%, 1:1.63 and sCAR-T = 75%, 1:1.89. (*E*) The phenotype of T cells in the peripheral blood from (*B* and *C*) after 21 d as the proportion of $CD3^+CD4/CD8^+$ by flow cytometry with staining for CD62-L and CD45RA ($n = 5$). Statistical significance was calculated using the one-tailed Student's *t* test (*B*, *C*, and *E*), where $^*P < 0.05$, $^{**}P < 0.01$, and $^{***}P < 0.001$; NS, not significant.

dosing of the LCNT switch was carried out every day for 10 d in the Nalm-6 model. At this low dose, tumor clearance was correspondingly slower compared with the conventional CART-19 and previous models, but still reached the limit of detection by the final day of dosing (day 16) (Fig. 5*D*). The Nalm-6 tumor relapsed in the 0.05-mg/kg treatment group at day 30 (15 d after the final dose), at which time the luciferase signal was significantly higher than for CART-19 treatment. These mice were retreated with a higher dose of the LCNT switch (0.5 mg/kg) for an additional 10 d. This retreatment regimen effectively decreased tumor signal to equivalent levels as CART-19 within 5 d and the mice remained tumor-free for >35 d after the final dose of the second treatment period. Thus, IgG4m sCAR-T cells in combination with an escalating switch-dose regimen can control cytokine release, while still providing efficacy comparable to conventional CART-19. This titration approach to reducing tumor burden with a lower initial dose of switch followed by increasing sCAR T-cell activity by escalating the switch dose may be an effective strategy for avoiding CRS in the clinic.

Persistent memory phenotypes have been correlated with complete remissions in CAR–T-cell therapy clinical trials for leukemia (38). To understand whether the switch dose can influence IgG4m sCAR–T-cell populations, we dosed NSG mice bearing the Nalm-6 tumor xenograft with 0.05-, 0.5-, or 2.5-mg/kg LCNT switch and analyzed the expression of CD45RA and CD62-L on $CD4^+$ and $CD8^+$ T cells in peripheral blood after 21 d (5 d after the final dose). The 2.5-mg/kg group demonstrated significant expansion of the $CD45RA^+CD62L^-$ terminal effector memory expressing CD45RA (TEMRA) compartment in both $CD4^+$ and $CD8^+$ T cells compared with the lower-dose groups (Fig. 5*E* and *SI Appendix*, Fig. S10*C*). Conventional CART-19 exhibited the greatest increase in TEMRA population, consistent with strong activation through the direct CAR design. Conversely, the lower-dose groups that received 0.05 and 0.5 mg/kg of switch had significantly larger populations of $CD45RA^-CD62L^+$ central memory cells compared with the 2.5-mg/kg group, which we hypothesize is a result of lower levels of stimulation during the initial dosing period. Thus, this result may indicate a potential benefit derived from low-dose treatment of sCAR-T cells during the initial stages of tumor clearance. Collectively, these results demonstrate that switch dose can control the activity, tissue-localization, cytokine release, and phenotype of sCAR-T cells in the Nalm-6 xenograft model with efficacy comparable to the corresponding conventional CART-19.

Discussion

We have demonstrated that protein engineering can be used to create antibody-based switches that redirect the activity of bioorthogonal anti-PNE sCAR-T cells to tumors. Moreover, we show this methodology allows one to systematically optimize the activity of the sCAR by varying the geometry and valency of the switch molecule. Similar approaches have been described using antibodies that are nonspecifically or enzymatically labeled with small-molecule haptens to redirect the activity antihapten CARs (16, 17). However, these systems do not easily allow for optimization of the immunological synapse between the CAR-T cell, antibody, and target cell. The importance of the spatial orientation between the T cell and target cell demonstrated in our studies is in agreement with several recent studies using conventional CARs, which showed that variation in the epitope location

of different targeting scFvs require compensatory CAR hinge designs for efficient CAR–T-cell activity (35, 36, 39, 40).

In the context of CD19 targeting, switches with the PNE engrafted at the N terminus (HCNT, LCNT, NTBV), proximal to the antigen-binding interface of FMC63, were found to be superior to switches with the PNE grafted at the C terminus (HCCT, LCCT, CTBV). Although the epitope of FMC63 and corresponding structure of the CD19 antigen are not known (41), we hypothesized that this trend was because of a decreased distance between the target cell and sCAR-T cell. In the case of the immunological synapse formed by the native T-cell receptor, the distance between the T cell and antigen presenting cell is reported to be ∼130–150 Å (42, 43). This distance is important to sterically exclude inhibitory phosphatases such as CD45 and CD148 from the synapse, which act to dephosphorylate signaling molecules and down-regulate T-cell activation (44). It is likely that the longer synapse resulting from the C-terminal switches (∼70 Å longer than the N-terminal switches) is unable to sterically exclude these inhibitory molecules, resulting in less-productive sCAR signaling. The increase in sCAR–T-cell activity observed when the sCAR hinge was shortened from 45 amino acids to 12 amino acids supports this hypothesis. A similar relationship was observed in the accompanying publication which reports a sCAR-T cell specific for FITC and a FMC63-based switch molecule that is site-specifically modified with FITC (45). FITC conjugation sites near the antigen-binding interface afforded better activity than sites distal to the binding interface. Moreover, we have shown, in that study, that nonspecific conjugation of switches with FITC did not provide sufficient in vivo activity to clear Nalm-6 tumor (45). Collectively, these studies underscore the importance of switch structure on optimizing immunological synapse geometry, which directly impacts sCAR–T-cell activity.

Switches based on the OFA antibody scaffold that target CD20 exhibited a trend similar to the FMC63 antibody when paired with sCAR-T cells harboring the CD8-based hinge. Interestingly, when the sCAR hinge was shortened to the 12-aa IgG4m hinge, the trend for OFA switches was reversed and C-terminal PNE switches afforded better activity than N-terminal switches. Although the structure of CD20 antibody is also unknown, the OFA antibody is reported to bind a small, membrane proximal loop of the multipass transmembrane CD20 antigen (31). In this case, it is likely that the distance created by the N-terminal OFA switches with the IgG4m sCAR is too short to enable efficient synapse formation between the sCAR and CD20. Alternatively, the large adjacent loop domain of the CD20 antigen may create a steric hindrance for binding of the IgG4m sCAR. We observed a similar effect supporting this hypothesis in our work with site-specific FITC conjugation on the anti-CD22 antibody m971 (45). In this case, the m971 antibody has a membrane proximal epitope on CD22 (39) and several large modular domains that may sterically preclude binding. Correspondingly, the m971 switches were optimal with FITC placed at sites distal from the antigen-binding interface. Thus, the geometry of the immunological synapse is a key parameter to consider when designing switches and highlights the requirement for precise control over switch structure, which cannot be accomplished with previously reported platforms.

A central tenant of the sCAR-T cells described here is the orthogonality of PNE-engrafted switches in that they only interact with the target cell and sCAR and no other immune receptors or cell types. Recently, Campana and coworkers reported a CD16 (Fc receptor)-based CAR-T cell for use in combination with therapeutic monoclonal antibodies (46). However, CD16 indiscriminately binds to therapeutic and naturally occurring antibodies, which yields the potential for any endogenous antibody to activate the CD16-CAR. This lack of orthogonality has the potential to cause off-target effects. Thus, in the development of orthogonal switches, Fabs may be desirable because their lack of an Fc domain removes the possibility of an Fc receptor-mediated off-target binding. In addition, the smaller size and shorter half-life of Fab molecules [∼12–20 h for Fab (47) vs. 10 d for IgG (48)] is also expected to provide better tumor penetration and greater temporal control over sCAR–T-cell activation in clinical translation. We expect this will correlate with every other day or twice a week dosing in the clinic.

To assess the efficacy of the sCAR–T-cell approach in vivo, we chose the Nalm-6 xenograft model. Because the Nalm-6 tumor lacks CD80 and CD86 coreceptors, it is difficult to treat and has become a standard for CAR-T therapy adjudication (49). Our sCAR–T-cell platform was able to eliminate Nalm-6 with comparable efficacy to conventional CART-19 T cells. Interestingly, differences in the in vitro lytic activity of switch/hinge designs that were generally less than 10-fold by EC_{50} were highly amplified for in vivo tumor elimination, reinforcing the need for careful in vitro design to provide robust in vivo activity. In addition to eliminating the tumor, in vivo expansion and trafficking of sCAR-T cells to sites of disease was demonstrated to be reliant on switch dosing. Conventional CAR–T-cell expansion and trafficking in human trials have been shown to be predictive of clinical responses (50). Importantly, serum levels of human cytokines IL-2, TNF-α, and IFN-γ were tightly controlled by LCNT switch dose. The exception was TNF-α, which was not increased in the 2.5-mg/kg group compared with the 0.5-mg/kg group, suggesting a potential maximum induction of this cytokine with 0.5 mg/kg LCNT; however, it is also possible that TNF-α in the 2.5-mg/kg group peaked earlier than 24 h, which was not captured in this experiment.

A key finding of this study was that sCAR-T cells treated with lower levels of LCNT switch (0.05 mg/kg) provided clearance of Nalm-6 at a slower rate and with lower levels of cytokine release. This finding suggests that low-dose switch treatment could be an effective method of mitigating CRS and TLS in the treatment of patients with high tumor burdens. When tumor relapsed at day 30, mice were retreated with a higher dose of 0.5 mg/kg to ensure clearance. Because of the lower tumor burden at this stage, excessive cytokine release would not be expected. The titration of sCAR–T-cell "on" activity to prevent CRS and TLS in the clinic would be a significant paradigm shift from proposed use of kill switches which can only turn "off" the CAR–T-cell response in the case of an adverse event (14).

Another key finding of the dose-titration study was the impact of switch dose on sCAR–T-cell phenotype. This experiment demonstrated a potential advantage to low-dose (0.05 mg/kg) switch treatment in its ability to maintain a larger CD62-L^+ central memory compartment compared with high-dose (2.5 mg/kg) treatment, which produced more TEMRA cells at day 21 (15 d after T-cell infusion). The formation of central memory CAR-T cells has been shown to provide prolonged persistence in clinical trials, and persistence has been correlated with sustained remissions for ALL and chronic lymphocytic leukemia patients (51, 52). In the sCAR–T-cell system, clinical persistence will also be critical to enable redosing strategies in the case of relapse. Thus, the ability to affect CAR–T-cell phenotype through dosing paradigms may be advantageous. We are currently exploring the impact of sCAR–T-cell phenotype on persistence in surrogate, syngeneic mouse models.

Toward translating sCAR-T cells to the clinic, we have initiated humanization and in silico prediction of T-cell epitopes for the murine 52SR4-based sCAR and FMC63-based switch to reduce the risk of development of human anti-mouse (HAMA) antibodies. We expect this will be important to ensure orthogonality of the sCAR–T-cell/switch interaction is not compromised by a HAMA response and to prevent immunological clearance of sCAR-T cells. Although the PNE sequence does not occur in the human proteome, it cannot be excluded that antigenic mimicry

could lead to off-target activation. Toward understanding this risk, we have initiated tissue cross-reactivity studies with the 52SR4 scFv.

In summary, sCAR-T cells represent a promising new paradigm in cell therapy that have the potential for improved safety and versatility compared with current T-cell therapies. We are currently testing sCAR-T cells in solid tumor models where the ability to titrate therapy to minimize organ toxicity due to shared antigen expression and bystander cellular toxicity may be critical (53). In addition, this added control over sCAR–T-cell activity may allow engineered cells to be turned off after tumor elimination to allow healthy B cells to repopulate in leukemia and lymphoma patients who are in remission. Indeed, in the companion article we show that switch discontinuation can lead to the restoration of the peripheral blood B cells in a surrogate mouse model using anti-FITC CAR-T cells and FITC labeled anti-murine CD19 switches (45). Finally, we expect that the ability of sCAR-T cells to target more than one antigen in vivo by codelivery of CD19 and CD20 switches may be an effective method to prevent relapse as a result of antigen-loss escape mutations in patients (11), and may provide improved efficacy in the treatment of cancers with heterogeneous antigen expression. Furthermore, the development of a single, universal sCAR-T cell is expected to obviate the development of a new CAR for each target and off-set the cost of cell therapy by standardizing vector design, cell manufacture, and treatment protocols across multiple indications.

Materials and Methods

Cell Lines and Human T Cells. RS4;11, Raji, and K562 cells were purchased from ATCC and cultured as per ATCC recommendations. Nalm-6 cells transduced with a GFP and firefly luciferase were kindly provided by R. Kochenderfer (National Cancer Institute) and cultured as per ATCC recommendations. Human T cells were obtained by Ficoll-Pacque purification of peripheral blood monocytes from normal donor whole blood from The Scripps Research Institute's Normal Blood Donor Service at Scripps General Clinical Research Center, under the appropriate The Scripps Research Institute's Institutional Review Board approval. Transduced CAR-T cells were subsequently cultured in Aim-V media supplemented with 5% (vol/vol) heat-inactivated human serum (Valley Biomedical) and 300 IU/mL of IL-2 (R&D Systems).

Cytotoxicity Assays. Cytotoxicity assays were carried out using the CytoTox 96 Non-Radioactive Cytotoxicity Assay (Promega). CAR-T cells were incubated with target cells at an effector: target cell ratio of 10:1, while maintaining a total cell concentration of 1×10^6/mL. The CAR-T cells used in these assays had a transduction efficiency of 50–75%, when different CAR designs were being compared mock-transduced cells were used to normalize the percentage of CAR^+ cells used in the assay. Switch was added to each well at a concentration of 1,000–0.01 pM and the cells were incubated for 37 °C for 20–24 h in complete RPMI with 5% (vol/vol) heat-inactivated FCS. LDH levels were measured in the assay supernatants as per the manufacturer's protocol: briefly, the maximum cell lysis was determined by target cell lysis using the 10% (vol/vol) cell lysis solution. Target cell cytotoxicity was calculated using the following formula: Cytotoxicity = 100 × [((sCAR-T cell + target cell + switch) – (sCAR-T cell + target cell))/(max target cell lysis – target cells alone)]. Cytokines in the cytotoxicity assay supernatants were analyzed using the Human Th1/Th2 Cytokine Bead Array kit II (CBA; BD). T-cell activation was measured using the cells from the cytotoxicity asasy, which were stained with anti-human CD3 (APC), anti-human CD25 (PE), and anti-human CD69 (PerCP) (Biolegend) and analyzed by flow cytometry to determine the proportion of $CD3^+$ T cells that were activated ($CD25^+$ $CD69^+$).

Xenograft Mouse Models. Female NOD.Cg-*Prkdc*^{scid} *Il2rg*^{tm1Wjl}/SzJ mice (NSG) mice, 9–11 wk of age, were purchased from Jackson Laboratories and maintained in the Calibr vivarium on a 12-h light cycle with access to food and water ad libitum. All protocols were approved by the Institutional Animal Care and Use Committee at Calibr. To carry out the xenograft models, NSG mice were inoculated with 5×10^5 luciferized Nalm-6 intravenously (day 0). On day 6, 40×10^6 CAR-T cells (50–75% CAR^+) were infused intravenously; unless otherwise stated, switches were dosed 6 h later. Mice were killed upon losing more that 15% of body weight or the development of hind limb paralysis. Graft vs. host disease was defined in indicated animals as hair loss, behavioral changes, and clear decrease in health not attributable to Nalm-6 luciferase signal. Tumor burden was measured by IVIS and was quantified as radiance in the region of interest, which was generally the area of one mouse. Fifty microliters of murine blood was drawn at 24 h and every 10 d after T-cell infusion (maximum of five times) to determine serum cytokine concentrations using the CBA kit, described above, and T-cell counts. T cells were analyzed in the blood of these mice at the stated time points by flow cytometry using: anti-CD3 (APC or PerCP), anti-CD4 (PerCP or PE/Cy7), anti-CD8 (PE or BV421), CD45RA (PE), or CD62-L (APC) (BioLegend), and were enumerated using the count bright beads (BD). T cells were defined as $CD3^+$ and either $CD4^+$ or $CD8^+$. Cells were analyzed using an LSR-II flow cytometer (BD).

Statistical Analysis. Statistical significance and EC_{50} values were calculated using GraphPad software. Unless otherwise stated, in vitro data were analyzed using the one-tailed Student's *t* test and in vivo data were analyzed by one-way ANOVA with Tukey's posttest or two-way ANOVA with Bonferroni's posttest. Data acquired from in vitro assays using experimental replicates are presented ± SD and data acquired in vitro or in vivo using biological replicates are presented ± SEM. $*P < 0.5$, $**P < 0.01$, and $***P < 0.001$.

Additional methods can be found in the *SI Appendix*.

ACKNOWLEDGMENTS. We thank Dr. James Kochenderfer for use of the luciferized Nalm-6 cell line, and Dr. Inder Verma for assistance with lentiviral constructs. This work was supported by National Institutes of Health Grant R01 GM062159-14 (to P.G.S.).

1. Sadelain M, Brentjens R, Rivière I (2013) The basic principles of chimeric antigen receptor design. *Cancer Discov* 3(4):388–398.
2. Kochenderfer JN, et al. (2013) Donor-derived CD19-targeted T cells cause regression of malignancy persisting after allogeneic hematopoietic stem cell transplantation. *Blood* 122(25):4129–4139.
3. June CH, et al. (2014) Engineered T cells for cancer therapy. *Cancer Immunol Immunother* 63(9):969–975.
4. Grupp SA, et al. (2013) Chimeric antigen receptor-modified T cells for acute lymphoid leukemia. *N Engl J Med* 368(16):1509–1518.
5. Uttenthal BJ, Chua I, Morris EC, Stauss HJ (2012) Challenges in T cell receptor gene therapy. *J Gene Med* 14(6):386–399.
6. Römer PS, et al. (2011) Preculture of PBMCs at high cell density increases sensitivity of T-cell responses, revealing cytokine release by CD28 superagonist TGN1412. *Blood* 118(26):6772–6782.
7. Xu XJ, Zhao HZ, Tang YM (2013) Efficacy and safety of adoptive immunotherapy using anti-CD19 chimeric antigen receptor transduced T-cells: A systematic review of phase I clinical trials. *Leuk Lymphoma* 54(2):255–260.
8. Brentjens R, Yeh R, Bernal Y, Riviere I, Sadelain M (2010) Treatment of chronic lymphocytic leukemia with genetically targeted autologous T cells: Case report of an unforeseen adverse event in a phase I clinical trial. *Mol Ther* 18(4):666–668.
9. Kalos M, et al. (2011) T cells with chimeric antigen receptors have potent antitumor effects and can establish memory in patients with advanced leukemia. *Sci Transl Med* 3(95):95ra73.
10. Lee DW, et al. (2015) T cells expressing CD19 chimeric antigen receptors for acute lymphoblastic leukaemia in children and young adults: A phase 1 dose-escalation trial. *Lancet* 385(9967):517–528.
11. Evans AG, et al. (2015) Evolution to plasmablastic lymphoma evades CD19-directed chimeric antigen receptor T cells. *Br J Haematol* 171(2):205–209.
12. Maude SL, et al. (2014) Chimeric antigen receptor T cells for sustained remissions in leukemia. *N Engl J Med* 371(16):1507–1517.
13. Straathof KC, et al. (2005) An inducible caspase 9 safety switch for T-cell therapy. *Blood* 105(11):4247–4254.
14. Di Stasi A, et al. (2011) Inducible apoptosis as a safety switch for adoptive cell therapy. *N Engl J Med* 365(18):1673–1683.
15. Wu CY, Roybal KT, Puchner EM, Onuffer J, Lim WA (2015) Remote control of therapeutic T cells through a small molecule-gated chimeric receptor. *Science* 350(6258):aab4077.
16. Tamada K, et al. (2012) Redirecting gene-modified T cells toward various cancer types using tagged antibodies. *Clin Cancer Res* 18(23):6436–6445.
17. Urbanska K, et al. (2012) A universal strategy for adoptive immunotherapy of cancer through use of a novel T-cell antigen receptor. *Cancer Res* 72(7):1844–1852.
18. Urbanska K, Powell DJ (2012) Development of a novel universal immune receptor for antigen targeting: To infinity and beyond. *OncoImmunology* 1(5):777–779.
19. Hanes J, Jermutus L, Weber-Bornhauser S, Bosshard HR, Plückthun A (1998) Ribosome display efficiently selects and evolves high-affinity antibodies in vitro from immune libraries. *Proc Natl Acad Sci USA* 95(24):14130–14135.

20. Mössner E, Koch H, Plückthun A (2001) Fast selection of antibodies without antigen purification: Adaptation of the protein fragment complementation assay to select antigen-antibody pairs. *J Mol Biol* 308(2):115–122.
21. Zahnd C, et al. (2004) Directed in vitro evolution and crystallographic analysis of a peptide-binding single chain antibody fragment (scFv) with low picomolar affinity. *J Biol Chem* 279(18):18870–18877.
22. Zola H, et al. (1991) Preparation and characterization of a chimeric CD19 monoclonal antibody. *Immunol Cell Biol* 69(Pt 6):411–422.
23. Bridgeman JS, Hawkins RE, Hombach AA, Abken H, Gilham DE (2010) Building better chimeric antigen receptors for adoptive T cell therapy. *Curr Gene Ther* 10(2):77–90.
24. Chen X, Zaro JL, Shen WC (2013) Fusion protein linkers: Property, design and functionality. *Adv Drug Deliv Rev* 65(10):1357–1369.
25. Liu T, et al. (2014) Rational design of CXCR4 specific antibodies with elongated CDRs. *J Am Chem Soc* 136(30):10557–10560.
26. Liu T, et al. (2015) Functional human antibody CDR fusions as long-acting therapeutic endocrine agonists. *Proc Natl Acad Sci USA* 112(5):1356–1361.
27. Zhang Y, et al. (2013) Functional antibody CDR3 fusion proteins with enhanced pharmacological properties. *Angew Chem Int Ed Engl* 52(32):8295–8298.
28. Milone MC, et al. (2009) Chimeric receptors containing CD137 signal transduction domains mediate enhanced survival of T cells and increased antileukemic efficacy in vivo. *Mol Ther* 17(8):1453–1464.
29. Zhang H, et al. (2007) 4-1BB is superior to CD28 costimulation for generating CD8+ cytotoxic lymphocytes for adoptive immunotherapy. *J Immunol* 179(7):4910–4918.
30. Zhang B (2009) Ofatumumab. *MAbs* 1(4):326–331.
31. Teeling JL, et al. (2006) The biological activity of human CD20 monoclonal antibodies is linked to unique epitopes on CD20. *J Immunol* 177(1):362–371.
32. Qin H, et al. (2015) Eradication of B-ALL using chimeric antigen receptor-expressing T cells targeting the TSLPR oncoprotein. *Blood* 126(5):629–639.
33. Aalberse RC, Schuurman J (2002) IgG4 breaking the rules. *Immunology* 105(1):9–19.
34. Classon BJ, et al. (1992) The hinge region of the CD8 alpha chain: Structure, antigenicity, and utility in expression of immunoglobulin superfamily domains. *Int Immunol* 4(2):215–225.
35. Hudecek M, et al. (2015) The nonsignaling extracellular spacer domain of chimeric antigen receptors is decisive for in vivo antitumor activity. *Cancer Immunol Res* 3(2): 125–135.
36. Hudecek M, et al. (2013) Receptor affinity and extracellular domain modifications affect tumor recognition by ROR1-specific chimeric antigen receptor T cells. *Clin Cancer Res* 19(12):3153–3164.
37. Barrett DM, et al. (2013) Regimen-specific effects of RNA-modified chimeric antigen receptor T cells in mice with advanced leukemia. *Hum Gene Ther* 24(8):717–727.
38. Terakura S, et al. (2012) Generation of CD19-chimeric antigen receptor modified CD8+ T cells derived from virus-specific central memory T cells. *Blood* 119(1):72–82.
39. Haso W, et al. (2013) Anti-CD22-chimeric antigen receptors targeting B-cell precursor acute lymphoblastic leukemia. *Blood* 121(7):1165–1174.
40. Jensen MC, Riddell SR (2015) Designing chimeric antigen receptors to effectively and safely target tumors. *Curr Opin Immunol* 33:9–15.
41. Grada Z, et al. (2013) TanCAR: A novel bispecific chimeric antigen receptor for cancer immunotherapy. *Mol Ther Nucleic Acids* 2:e105.
42. Srivastava S, Riddell SR (2015) Engineering CAR-T cells: Design concepts. *Trends Immunol* 36(8):494–502.
43. Wang R, Natarajan K, Margulies DH (2009) Structural basis of the CD8 alpha beta/MHC class I interaction: Focused recognition orients CD8 beta to a T cell proximal position. *J Immunol* 183(4):2554–2564.
44. Chakraborty AK, Weiss A (2014) Insights into the initiation of TCR signaling. *Nat Immunol* 15(9):798–807.
45. Ma J, et al. (2015) Versatile strategy for controlling the specificity and activity of engineered T cells. *Proc Natl Acad Sci USA* 113:E450–E458.
46. Kudo K, et al. (2014) T lymphocytes expressing a CD16 signaling receptor exert antibody-dependent cancer cell killing. *Cancer Res* 74(1):93–103.
47. Flanagan RJ, Jones AL (2004) Fab antibody fragments: Some applications in clinical toxicology. *Drug Saf* 27(14):1115–1133.
48. Wang W, Wang EQ, Balthasar JP (2008) Monoclonal antibody pharmacokinetics and pharmacodynamics. *Clin Pharmacol Ther* 84(5):548–558.
49. Brentjens RJ, et al. (2007) Genetically targeted T cells eradicate systemic acute lymphoblastic leukemia xenografts. *Clin Cancer Res* 13(18 Pt 1):5426–5435.
50. Kalos M, June CH (2013) Adoptive T cell transfer for cancer immunotherapy in the era of synthetic biology. *Immunity* 39(1):49–60.
51. Li XC, Kloc M, Ghobrial RM (2013) Memory T cells in transplantation—Progress and challenges. *Curr Opin Organ Transplant* 18(4):387–392.
52. Riddell SR, et al. (2014) Adoptive therapy with chimeric antigen receptor-modified T cells of defined subset composition. *Cancer J* 20(2):141–144.
53. Morgan RA, et al. (2010) Case report of a serious adverse event following the administration of T cells transduced with a chimeric antigen receptor recognizing ERBB2. *Mol Ther* 18(4):843–851.